RESEARCH REPORT

LOW TURBULENCE WIND TUNNEL OF NAGOYA UNIV.

YOSHIMASA FURUYA, HIDEO OSAKA and TAKEHIRO KUSHIDA

Department of Mechanical Engineering

(Received May 24, 1971)

1. Introduction

In general, an experimental proof with exact measurements is very important for the systematic study of turbulent boundary layers.

Fig. 1 shows the range of the Reynolds number for some transport machines (a ship, trains and an aeroplane) recently used, where the values of the Reynolds number referring to the length along the flow are over 10^7 to 10^9 which should be regarded as necessary for model tests of boundary layers. As the surface in practical application is almost rough, it is considered to be sufficient when the Reynolds number of test facilities is about 5×10^5 to 10^6. But even so, the size of the apparatus should become considerably large, if we use a wind tunnel of the common type.

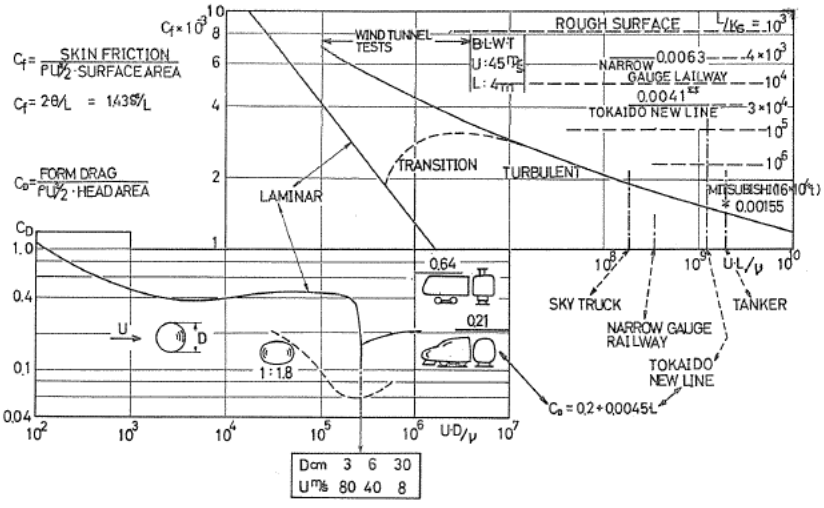

FIG. 1. Skin friction coefficients and Drag coefficients for some transport machines.

Meanwhile, the ratio of the velocity fluctuation u' to the main flow velocity U in the flow around the body which moves in a free air or water is about 0.05%,

then this value will be require for the flows in the wind tunnel. Therefore, a special type of low turbulence wind tunnel having the test section sufficiently long and with equipments for adjusting the pressure gradient is required to study the boundary layer in practice.

In this paper, we describe the low turbulence boundary layer tunnel equipped at the Hydraulic Laboratory in Nagoya University and its performances.

Nomenclatures

x: distance from the leading edge of the measuring plate
y: distance from the plate
z: distance in spanwise direction from the center line
u: x component velocity in boundary layer
U: velocity outside the boundary layer
u': root mean square value of velocity fluctuation in x direction
Px: pressure on the plate
Pa: atmospheric pressure
P_f-P_r: preseure difference between the front and rear points of the turbulence sphere
δ^*: displacement thickness
θ: momentum thickness
H: shape factor $(=\delta^*/\theta)$
D: friction
G: Clauser's form parameter
C_f: total skin friction coefficient
$Rx=U\cdot x/\nu$
$Rd=U\cdot d/\nu$
d: diameter of sphere

2. Experimental Equipment and Techniques

2-1. Wind tunnel

Fig. 2 gives a description of the wind tunnel of a closed curcuit type, with a full length of about 17.5 m and a contraction ratio of 1/12.5, and made in steel.

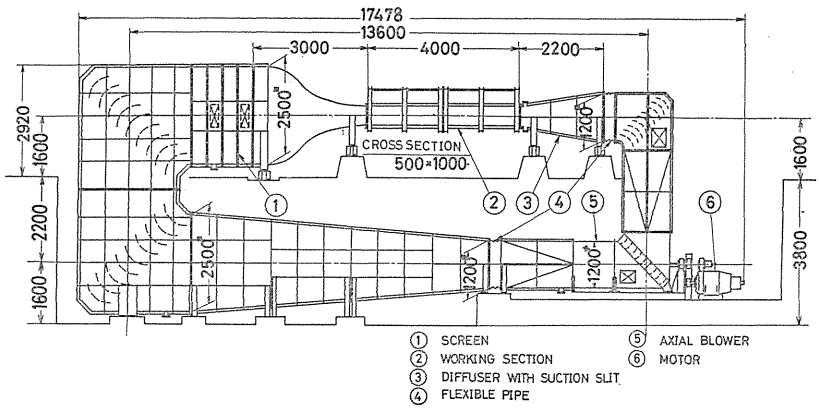

FIG. 2. Low turbulence wind tunnel.

The working section is 0.5 m × 1 m × 4 m where the wind speed is 10 to 50 m/s. The settling chamber contains 5 screens of 20 to 60 mesh in order to decrease the turbulence level of flow down-stream from them. The chord vanes in each four corners take the form of simple combined circular-arc with straight line.

2–2. Working section

The working section is of closed type and of 0.5 m × 1 m of rectanglar cross section with 4 m long. The roofs of the working section can be adjusted in order to impose any desired pressure gradient upon the floor on which measurements are made. Side walls are constructed by transparent plates of Acrinol resin in order to observe the inner situation.

The floor contains a measuring flat plate of 2 m long with its leading edge located 965 mm downstream from the entrance of the working section. As shown in Fig. 3 (Pt. B), this measuring plate can be adjusted up and down, according as the measurements are performed on the surface skin friction or turbulence intensity respectively. At the leading edge of the plate, boundary layer suction is applied to remove boundary layers developed upstream of the plate.

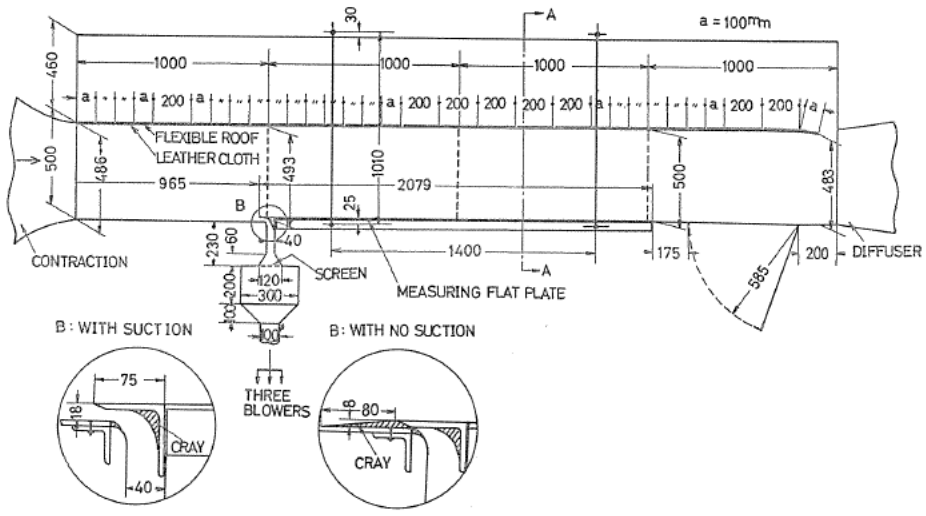

FIG. 3. Working section.

2–3. Attachments

a. Equipments for adjusting static pressure on the measuring plate

As shown in Fig. 3 and Fig. 4, the roof are made up of slats, which are constructed by a number of Alminium plates connected with each other by hinges. Each slats can be adjusted by means of jacking screws to give the desired roof shape, then the cross sectional area and static pressure on the measuring plate can be changed. In order to preserve the smooth surfaces and to stop a leak air, the leather clothes were stuck on the inner side of the roof slats.

b. Equipments for boundary layer suction

As shown in Fig. 3 (Pt. B), the boundary layers developed upstream of the leading edge are drawn by three blowers, then, the boundary layer develops just

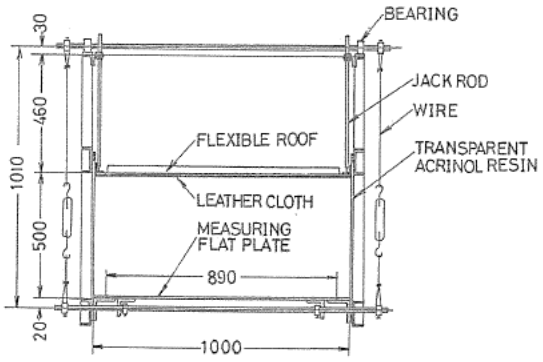

FIG. 4. Cross section of a working section at A-A.

from the leading edge of plate and the two-dimensionality of boundary layer flow can be obtained.

c. Direct measurements of friction drag

The Equipment is shown in Fig. 4 and Fig. 5; Measuring plate is hung by wires and can be moved rearward by friction of flow. The movement of the plate is measured by means of strain gauge as shown by Fig. 5. Using the calibrated relations between drag and the movement, friction drag of the plate can be estimated from the movement measured by the strain gauge.

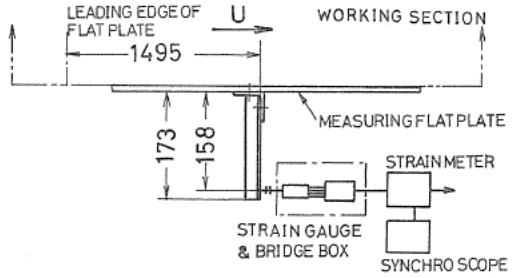

FIG. 5. Instruments for direct measurement of skin friction.

d. Turbulence sphere

Using the turbulence sphere (Fig. 6 (a)), the critical Reynolds number of a sphere is decided as the value of the Reynolds number at which the pressure difference between the forward stagnation point and the position inclined at an angle of 22.5° with respect to the rear axis decreases rapidly, as the Reynolds number increases. Then the ratio of this critical Reynolds number to the value in free air of 3.85×10^5, that is, the turbulence factor determines the turbulence intensity by means of a curve of Fig. 6 (b).

3. Results of Experiments

3-1. Turbulence intensity

a. Turbulence intensity determined by means of the turbulence sphere

The pressure difference between the front and rear holes of the turbulence

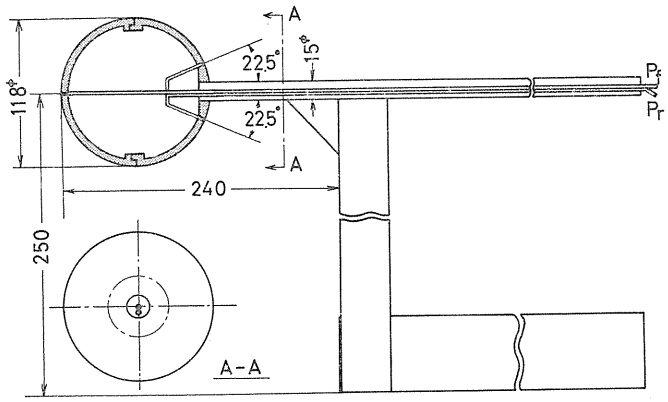

FIG. 6 (a) Turbulence sphere.

sphere, is plotted against Reynolds number $U \cdot d/\nu$ where d is the diameter of the sphere. The critical Reynolds number at which the pressure difference changes rapidly is somewhat different in the case when wind speed increases and when it decreases as shown in Fig. 7 (a) and (b) respectively. The result of critical Reynolds numbers are 3.53×10^5 and 3.41×10^5 respectively according to Fig. (a) and (b). Then the turbulence intensity which is determined by the curve of Fig. 6 (b) are 0.12% and 0.15% respectively. The main flow speed at this critical Reynolds number is 40 m/s. We measured also the turbulence intensity at that speed by means of hot wire instrument. The results due to the hot wire is 0.13% which agrees very well with the results by turbulence sphere.

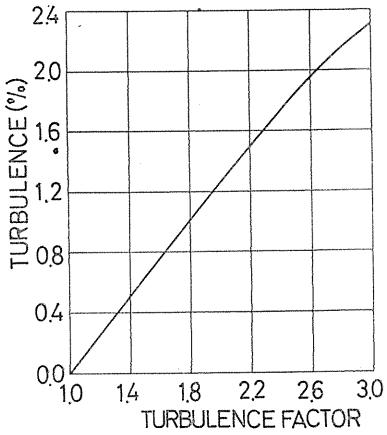

FIG. 6 (b) The variation of the turbulence factor with turbulence.

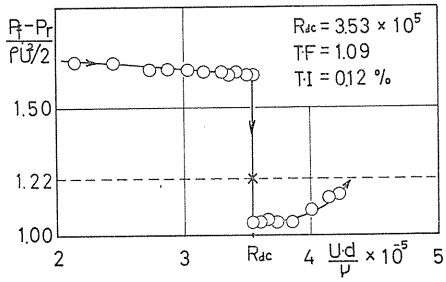

FIG. 7 (a) Pressure difference in the case of increasing wind speed.

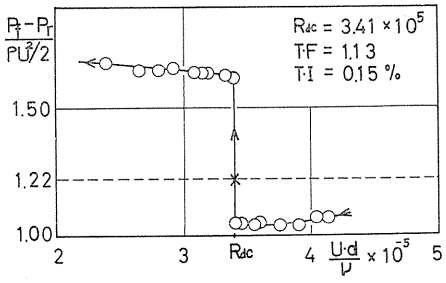

FIG. 7 (b) Pressure difference in the case of decreasing wind speed.

b. Turbulence intensity determined by means of hot wire anemometer

Turbulence intensity distribution in a cross section at $x=1332$ mm from the leading edge of the measuring plate, are shown in Fig. 8 where the main velocity U is 30 m/s and 35 m/s respectively. Figures in the graph show the values of the percent ratio of the root mean square of turbulent velocity u' to the time mean velocity U. When $U=30$ m/s, the value of turbulence intensity is 0.05% in a greater part of central region of the cross section and does not exceed 0.10% even in a more wide region. When $U=35$ m/s, the turbulence intensity is 0.10% in the central region of the cross section and is 0.15% in a more wide region. As the velocity increases to 40 m/s or decreases to 20 m/s, the turbulence intensity increases slightly.

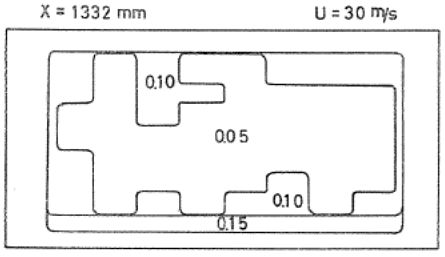

FIG. 8-1

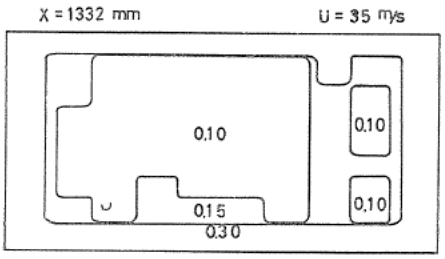

FIG. 8-2

FIG. 8. Turbulence intensity distribution in a cross section at $X=1332$ mm in the case of $U=30$ and 35 m/s.

3-2. Velocity distribution in the working section

Fig. 9 shows the velocity distribution in a cross section in the working section measured in the same positions and at the speeds as Fig. 8. In the case of $U=30$ m/s, velocity distribution is almost uniform over the cross section with the exception of small parts in a cross section where the velocity variation is $\pm 2.5\%$. When $U=35$ m/s, velocity distribution becomes more uniformly. Even if the speed changes to 20 m/s, 25 m/s and 40 m/s, results were almost the same as the above one. Figures in the graph show the values of the percent ratio of local time mean velocity to the value at the central parts of the cross section.

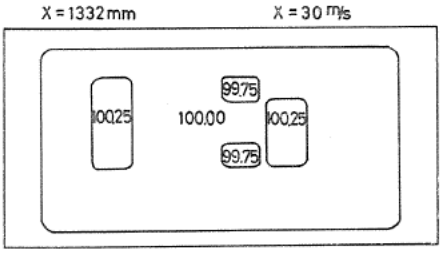

FIG. 9-1

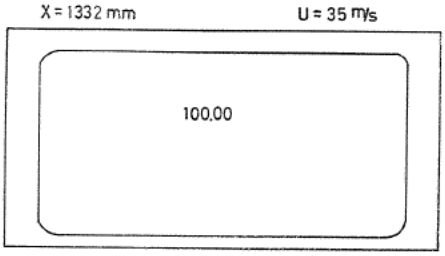

FIG. 9-2

FIG. 9. Velocity distribution in a cross section at $X=1332$ mm in the case of $U=30$ and 35 m/s.

3-3. Turbulent boundary layer on the flat plate

Fig. 10 shows the velocity distribution of turbulent boundary layers on the

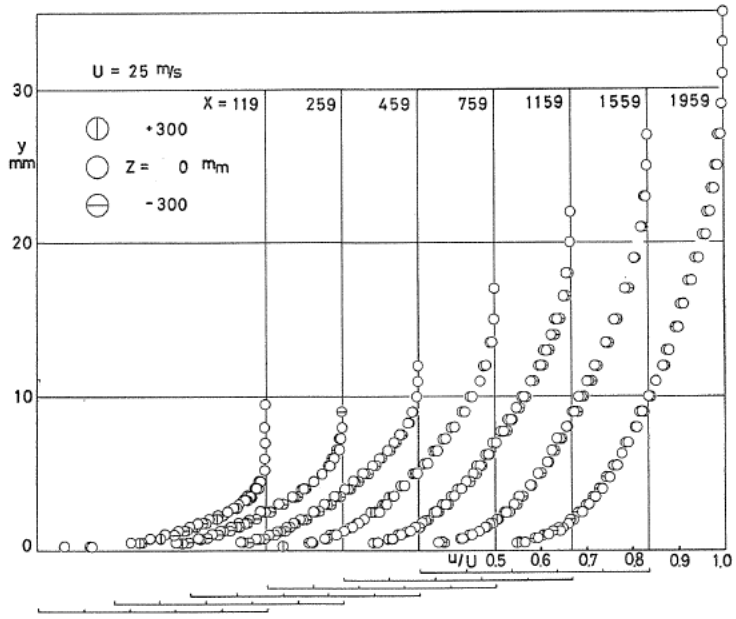

FIG. 10-1

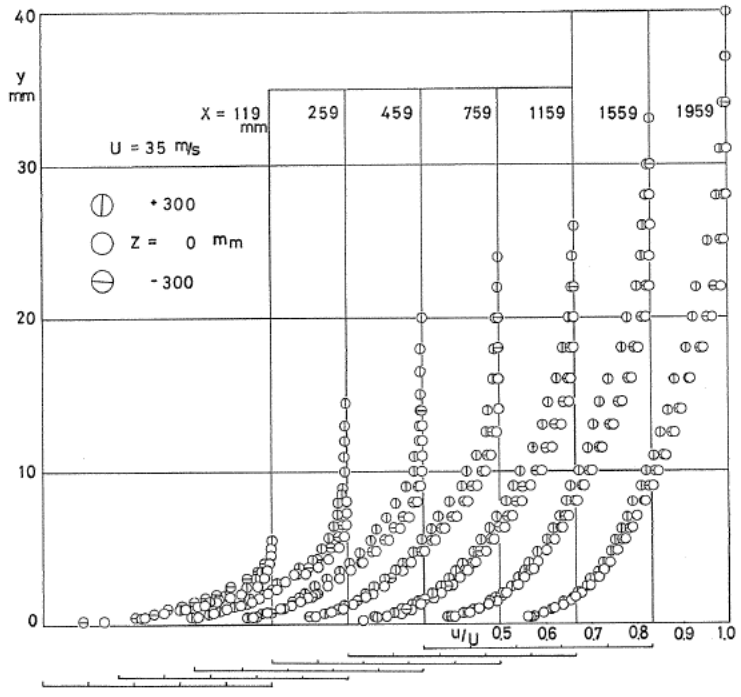

FIG. 10-2

FIG. 10. Velocity profile of turbulent boundary layer on a flat plate in the case of U=25 m/s and 35 m/s.

flat plate in the case of $U=25$ m/s and 35 m/s, when the tripping wire is laid at the leading edge. Measurements are carried out on the wall along the three longitudinal lines, $Z=0$, $+300$ and -300 mm respectively in cross sections of $X=$ 119, 259, 459, 759, 1159, 1559, and 1959 mm, where X is a distance from the leading edge. In the case of $U=25$ m/s, the flow is nearly two-dimensional since velocity ratio u/U does not change in the Z direction. But at $U=35$ m/s and 40 m/s, the two-dimensionality fails slightly.

Pressure distribution along the flow is shown in Fig. 11. In this figures non-dimensional pressure difference $(Px-Pa)/\frac{1}{2}\rho U^2$ are plotted against X, where Px is pressure at the measuring point and Pa atmospheric pressure.

In Fig. 12, shape factor of the velocity profile $H=\delta^*/\theta$ (δ^*: displacement thickness, θ: momentum thickness) is plotted versus X. As is evident in Fig. 12,

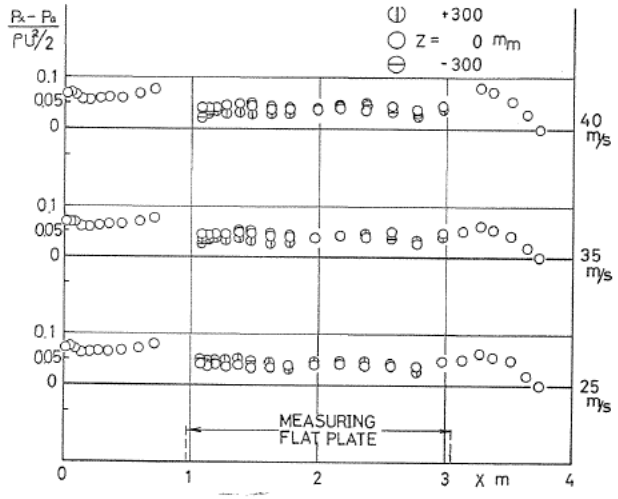

FIG. 11. Pressure distribution along the flow.

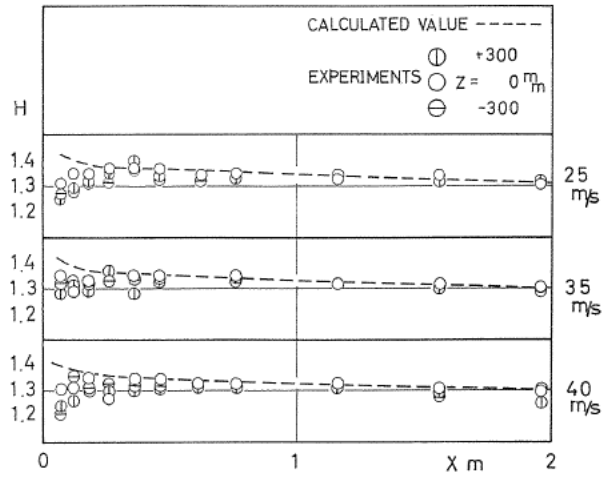

FIG. 12. Shape factor H of the velocity profile.

the value of shape factor decreases linearly from about 1.35 at $X=300$ mm to about 1.30 at trailing edge in the case of $U=25$ m/s, 35 m/s and 40 m/s respectively. Excepting for the vicinity of leading edge of the plate, values of shape factor are in good agreement with the values calculated from Clauser's equation

$$H=\frac{1}{1-G\sqrt{\frac{C_f}{2}}} \tag{1}$$

where $G=6.1$ in zero pressure gradient, which is plotted by a broken line in Fig. 12.

3-4. Total skin friction coefficient

When pressure along the flow is constant, total skin friction coefficient C_f can be determined from the velocity profile and is given by

$$C_f=D\Big/\frac{1}{2}\rho U^2\cdot X=\frac{2\cdot\theta}{X} \tag{2}$$

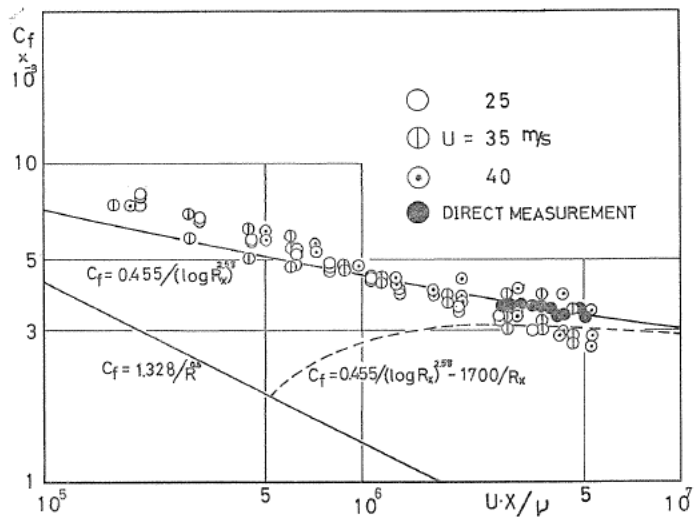

FIG. 13. Total skin friction coefficients of the flat plate with smooth surface.

where D is the friction drag of flow exerted upon a flat plate. It is seen from Fig. 13 that the values of total skin friction coefficient are nearly the same as the Prandtl-Schlichting's equation excepted for vicinity of the leading edge. And also, the values of skin friction coefficient obtained from the direct measurements of wall shear stress, which is plotted by a black dot in Fig. 13, are in agreement with Prandtl-Schlichting's equation.

4. Conclusion

From the results mentioned above, it may be right to consider that this wind tunnel has an extensive usefulness for experimental researches for boundary

layers.

A part of this research was supported by scientific research fund from the Ministry of Education.

References

1) T. Shigemi and K. Hirooka, J. JSASS, **15** (1967), 167.
2) P. Bradshaw and G. E. Hellens, ARC R. and M., **3437** (1964).
3) H. L. Dryden and G. B. Schubauer and *et al.*, NACA Rep., **581** (1937).